JOURNAL OF MATERIALS SCIENCE 30 (1995) 6309–6315

Elevated temperature deformation of several quaternary $L1_2$ Al_3Ti based alloys reinforced with TiB_2 particles

J. D. WHITTENBERGER
NASA Lewis Research Center, 21000 Brookpark Road, Cleveland, OH, 44135 USA
K. S. KUMAR, M. S. DIPIETRO, S. A. BROWN
Martin Marietta Laboratories, Baltimore, MD, 21227 USA

Concurrent with an investigation of quaternary cast and forged $L1_2$ modified Al_3Ti's containing 9 at% Cr, Fe and/or Mn, a similar series of four alloys was produced via XD™ technology, whereby 20 vol% of ~ 0.5 μm TiB_2 particles was incorporated as a reinforcement. Following densification by hot pressing and slow isothermal forging, small diameter compression test samples were machined from each compact and tested. The 0.2% yield strength measurements revealed a strength advantage for the particulate reinforced materials over the unreinforced ingot metallurgy matrices to about 1175 K. Furthermore, 900 and 1100 K constant velocity testing indicated that the TiB_2 containing materials were stronger than the ingot metallurgy matrices down to strain rates of $\sim 10^{-7} s^{-1}$. None of the quaternary $L1_2$ alloys + 20 TiB_2 consistently displayed a strength advantage over others. However, extrapolation of the present mechanical property data into slower strain regimes indicated that the composites will not possess any strength advantage over the unreinforced versions. Such losses in strength appeared to be caused by small grains in the particulate reinforced alloys, which promoted grain boundary weakening mechanisms.

1. Introduction

$L1_2$ modified Al_3Ti has been proposed [1] as a possible high temperature structural material useable to perhaps 1200 K in part due to

1. its existence over a range of compositions [2], as opposed to the line compound nature of Al_3Ti;
2. the inherently more ductile cubic $L1_2$ crystal structure, instead of the brittle DO_{22} base;
3. its very high Al content, which imparts excellent oxidations resistance [3] compared to Ti rich alloys or intermetallics.

Two major areas of concern, however, still exist for the $L1_2$ modified Al_3Ti alloys. First, with the exception of an Mn containing alloy (Al_{66} Ti_{25} Mn_9, [4]) none of the other versions of $L1_2$ modified Al_3Ti consistently display any room temperature tensile ductility. Second, the yield strength of cast monolithic materials between room temperature and 1200 K is relatively low ($\sim$ 300 MPa) and the creep resistance of such alloys rapidly diminishes at or above 1000 K [5].

In an attempt to improve the strength, Kumar and coworkers [6–8] investigated a powder metallurgy (PM) approach involving XD™ synthesis to fabricate fine grain sized $L1_2$ modified Al_3Ti alloys containing up to 20 vol% TiB_2 particles. This method led to remarkable improvements in yield strengths with values approaching 2000 MPa for alloys containing 20 vol% of the diboride. Testing as a function of temperature, however, revealed that such improvements in yield strength could only be maintained to about 900 K. Furthermore, creep testing of the composites indicated that their strength fell rapidly with decreasing strain rate to the point where, in many cases, the small grain size PM materials with TiB_2 were weaker than unreinforced matrices produced by ingot metallurgy (IM) techniques. Based on previous work [9] with XD™ processed TiB_2–NiAl composites, such a loss in creep resistance was unexpected.

Concurrent with an IM study [10–12] to improve the room temperature ductility and elevated temperature creep resistance by multiple element alloying, XD™ synthesis in combination with PM techniques was utilized to fabricate particulate TiB_2 versions of the same quaternary alloys. Direct comparison of the mechanical properties of the various materials would then allow another test of the influence of TiB_2 particles on strength. The purpose of this paper is

1. to document the compressive yield strength and time dependent flow strength properties of the four quaternary $L1_2$ modified Al_3Ti based materials reinforced with 20 vol% TiB_2 particles, and
2. to compare their properties to those for the unreinforced ingot metallurgy matrices.

0022–2461

2. Experimental procedure

Elemental powders (≤ 150 μm) were mixed together to yield the following four chemistries: $Al_{66}Ti_{25}Cr_{4.5}Fe_{4.5}$, $Al_{66}Ti_{25}Cr_{4.5}Mn_{4.5}$, $Al_{66}Ti_{25}Fe_{4.5}Mn_{4.5}$ and $Al_{66}Ti_{25}Mn_{6.7}Fe_{2.3}$. Each of these mixtures was then blended with sufficient excess Ti and submicrometre B powder to produce 20 vol % TiB_2 when reacted. The blends were cold isostatically pressed, processed by XD™ synthesis and ground into powder. In an effort to reduce the amount of entrapped oxide found when ≤ 63 μm diameter ground particles were densified [13], a distribution of powder from the XD™ processing was chosen for densification, where 50% of the diameters lie between 150 to 90 μm, 10% between 90 and 44 μm and the remaining fraction composed of diameters smaller than 44 μm. The use of this non-Gaussian distribution led to difficulties in densification, since significant porosity was still noted after a 2 h vacuum hot pressing at 1498 K at 20 MPa, followed by hot isostatic pressing at 1473 K at 200 MPa for 4 h. Hence, the partially consolidated materials were slowly forged to $\sim 50\%$ at 10^{-3} mm s^{-1} and 1473 K to close the porosity. Lastly to be consistent with the four IM quaternary alloys [11], the forged materials were given a two step homogenization treatment in Ar: 24 h at 1323 K followed by 96 h at 1473 K.

After homogenization small cylindrical compression specimens (5.1 mm in diameter by 10.9 mm tall) were wire electrodischarged machined (EDM) from each of the four materials, with the long sample axis parallel to the hot pressing (forging) direction. Compressive yield strength was measured at a strain rate of 10^{-4} s^{-1} from 77 to 1273 K with testing at 293 K and above being conducted in air, while lower temperature experiments were undertaken by immersion in a methanol–dry ice mixture (205 K) or liquid nitrogen (77 K). Stress–strain–strain rate properties were determined between 900 and 1100 K in air through constant velocity testing in a universal test machine operating at speeds from 2.1×10^{-2} to 2.1×10^{-6} mm s^{-1}. All testing was conducted on samples with as-EDMed surface finishes, strains were calculated by the offset method applied to the autographically recorded load–time charts, and stresses were computed assuming conservation of volume.

Metallographic sections of each of the homogenized forgings and selected compression tested samples were examined in both the unetched and etched states. Exact chemical compositions of the materials were not determined; however, based on previous work [6, 8, 13] with ternary XD™ processed $L1_2$ modified Al_3Tis alloys containing from 0 to 20 vol % TiB_2, the final compositions were generally close to the desired chemistries.

3. Results

The 0.2% compressive yield strengths of the four quaternary $L1_2$ modified Al_3Ti alloys reinforced with 20 vol % TiB_2 are presented in Fig. 1 as a function of temperature. While the data illustrate that the composites are relatively strong, a degree of scatter can be found in these results, where no one material consistently displays stronger or weaker characteristics. From 77 and 800 K, the data lie in a band between 1000 and 1200 MPa; at higher temperatures, however, the alloys with TiB_2 become progressively weaker and the width of the band significantly narrows.

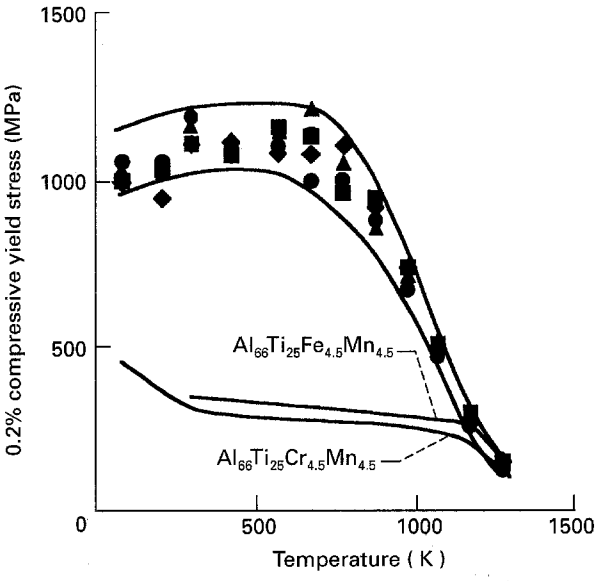

Figure 1 Compressive yield strengths of four quaternary $L1_2$ matrix composites containing 20 vol % TiB_2 particles and two ingot metallurgy versions of the matrices as a function of temperature (IM results from [10]). (■) $Al_{66}Ti_{25}Cr_{4.5}Fe_{4.5}$ + 20 TiB_2, (◆) $Al_{66}Ti_{25}Cr_{4.5}Mn_{4.5}$ + 20 TiB_2, (▲) $Al_{66}Ti_{25}Fe_{4.5}Mn_{4.5}$ + 20 TiB_2, (●) $Al_{66}Ti_{25}Mn_{6.7}Fe_{2.3}$ + 20 TiB_2.

True compressive stress–strain curves for the particulate reinforced quaternaries tested at 1000 K are plotted in Fig. 2 as a function of the nominal strain rate. Irrespective of the imposed rate, all the materials exhibit rapid work hardening through the first 1% of deformation. At the fastest strain rate ($\sim 2.1 \times 10^{-4}$ s^{-1}) the materials continue to work harden, albeit at a much reduced rate, throughout the duration of the test; while at lower strain rates flow either continues at a more or less constant stress (2.1×10^{-5} s^{-1}) or reaches a diffuse peak and is followed by softening (2.1×10^{-6} s^{-1}). Stress–strain diagrams from constant velocity testing of the materials at 900 and 1100 K are presented in Fig. 3. These plots are consistent with those of Fig. 2, where rapid work hardening occurs through $\sim 1\%$ strain. Behaviour at higher strain values is dependent on the imposed conditions, where deformation at 900 K at 2.1×10^{-5} s^{-1} leads to continuous work hardening, while slower strain rates at 900 or any 1100 K testing gives a constant, or slowly decreasing, flow stress.

As can be envisioned from Figs 2 and 3, the strength of each material is dependent on the imposed deformation rate and temperature. The reliance of strength on strain rate, $\dot{\varepsilon}$, and temperature, T, is shown in Fig. 4, where flow stresses, σ, were evaluated from the stress–strain diagrams at 1% strain. Two equations were utilized to describe these data: at the slower rates a temperature compensated power law was utilized, Equation 1; while at faster rates a temperature

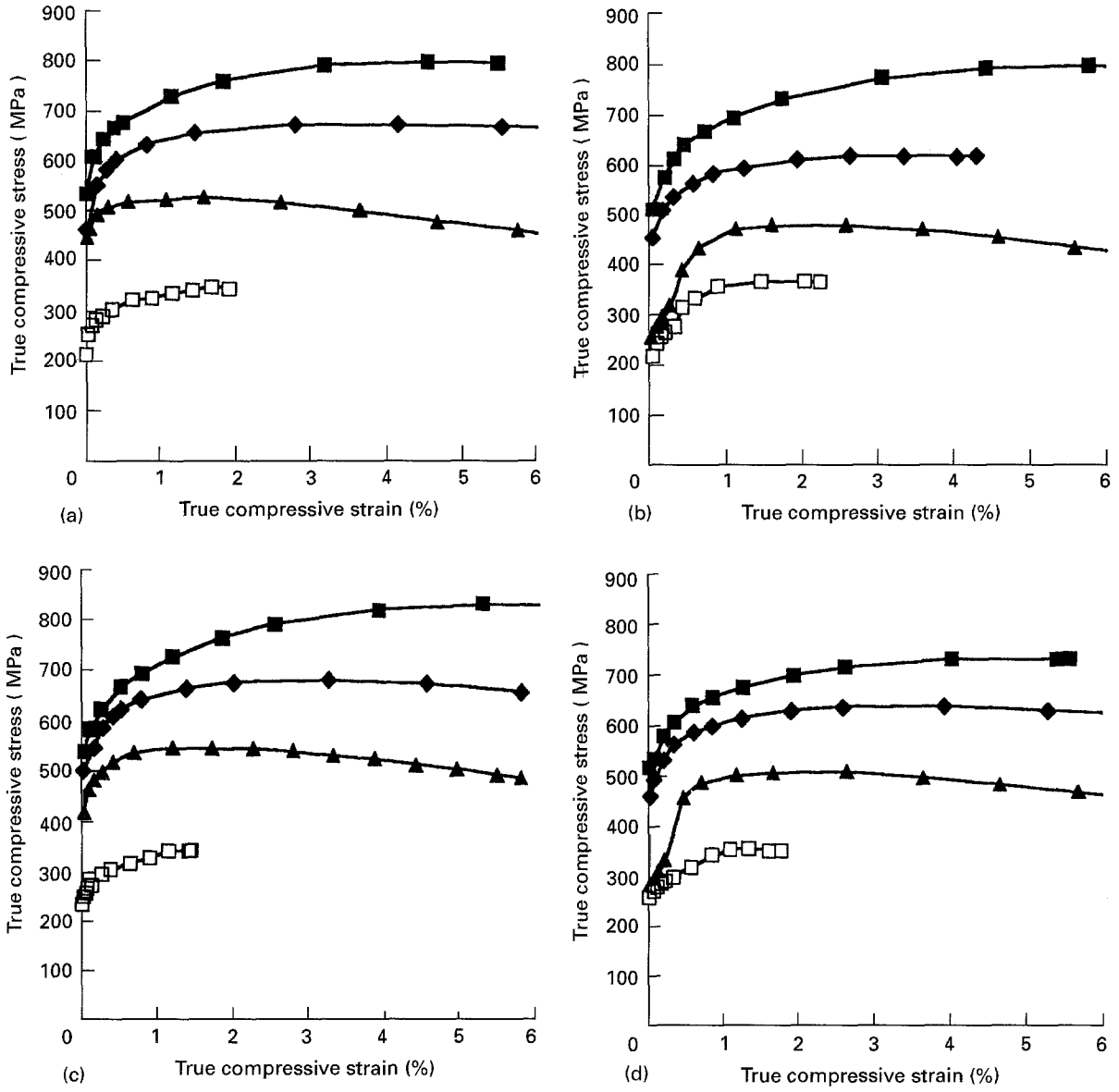

Figure 2 True compressive stress–strain diagrams for the composites tested under constant velocity conditions at 1000 K: (a) $Al_{66}Ti_{25}Cr_{4.5}Fe_{4.5}$ + 20 TiB_2, (b) $Al_{66}Ti_{25}Cr_{4.5}Mn_{4.5}$ + 20 TiB_2, (c) $Al_{66}Ti_{25}Fe_{4.5}Mn_{4.5}$ + 20 TiB_2, and (d) $Al_{66}Ti_{25}Mn_{6.7}Fe_{2.3}$ + 20 TiB_2 at approximate strain rates of (■) 2.1×10^{-4}, (◆) 2.1×10^{-5}, (▲) 2.1×10^{-6}, and (□) $2.1 \times 10^{-7}\ s^{-1}$.

compensated exponential law, Equation 2, was invoked

$$\dot{\varepsilon} = A\sigma^n \exp(-Q/RT) \quad (1)$$

$$\dot{\varepsilon} = C\exp(D\sigma)\exp(-Q/RT) \quad (2)$$

where A, C and D are constants, n is the stress exponent, Q is the activation energy for deformation and R is the universal gas constant. Results from linear regression analyses are shown in Fig. 4, where the solid lines indicate the extent of the power law fits, and dash lines outline the limits of the exponential law fits. Since only one 1100 K data point was available for $Al_{66}Ti_{25}Cr_{4.5}Mn_{4.5}$ + 20TiB_2 (Fig. 4b), just the exponential law, Equation 2, was utilized to describe this material. A listing of the values for the parameters in Equations 1 and 2, as well as the coefficient of determination, R_d^2, and the standard deviations, δ_i, for the deformation parameters i are given in Table I (a) and (b). Compared to previous work, the values of about five for the stress exponents and $\sim 400\ kJ\ mol^{-1}$ for the power law activation energies are similar to those calculated for a number of Cr, Fe and Mn base $L1_2$ modified Al_3Ti alloys reinforced with 20 vol % TiB_2 [6, 7].

Although the temperature compensated exponential law, Equation 2, was chosen to fit the lower temperature–higher strain rate data in Fig. 4, these results could also be fitted to the usual temperature compensated power law, Equation 1. The results from such calculations are given in Table I (c). Comparison of the fits resulting from use of the two expressions, Table I(b) and (c), reveals that both equations give similar activation energies for each material. In terms of description of the data as denoted by R_d^2, the temperature compensated exponential law, Equation 2, fits $Al_{66}Ti_{25}Cr_{4.5}Fe_{4.5}$ and $Al_{66}Ti_{25}Cr_{4.5}Mn_{4.5}$ better than temperature compensated power law, Equation 1; while both Equations 1 and 2 yield similar characterizations of $Al_{66}Ti_{25}Fe_{4.5}Mn_{4.5}$ and $Al_{66}Ti_{25}Mn_{6.7}Fe_{2.3}$. Finally, use of the temperature compensated power law description of the flow stress–strain

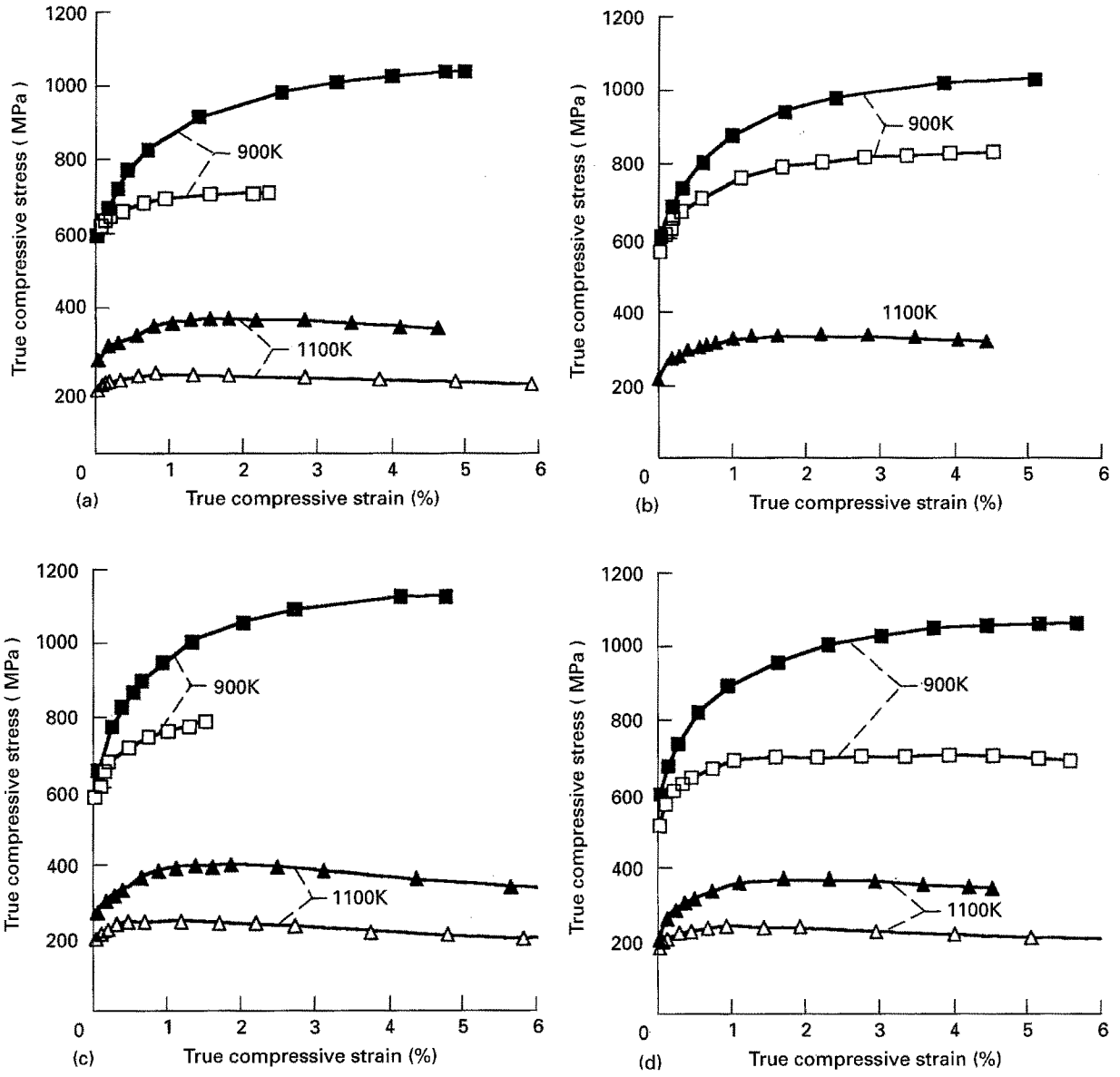

Figure 3 True compressive stress–strain diagrams for the composites tested under constant velocity conditions at 900 and 1100 K: (a) $Al_{66}Ti_{25}Cr_{4.5}Fe_{4.5}$ + 20 TiB_2, (b) $Al_{66}Ti_{25}Cr_{4.5}Mn_{4.5}$ + 20 TiB_2, (c) $Al_{66}Ti_{25}Fe_{4.5}Mn_{4.5}$ + 20 TiB_2, and (d) $Al_{66}Ti_{25}Mn_{6.7}Fe_{2.3}$ + 20 TiB_2 at approximate strain rates of (■) 2.1×10^{-5}, (□) 4.2×10^{-7}, (▲) 2.1×10^{-5}, and (△) 2.1×10^{-6}.

rate results for the particulate reinforced quaternaries indicates that the stress exponents in the lower temperature–higher strain rate regime, Table I (c), are two to three times larger than those in the higher temperature–slower strain rate region, Table I (a).

Two typical microstructures observed after compression testing are presented in Fig. 5. The structure away from the sample surfaces was identical to that seen in the untested materials, where oxide particles (dark gray) from the PM processing are scattered throughout the microstructure in unetched samples (Fig. 5a), and a mottled structure composed of dark and light areas is found after etching (Fig. 5b). Based on microstructural studies of $Al_{67}Ti_{25}Cr_8$ and $Al_{66}Ti_{25}M_9$ reinforced with 20 vol % TiB_2, the dark regions consisted of micrometre sized grains of $L1_2$ modified Al_3Ti and a high density of ~ 0.5 μm square cross-section TiB_2 particles; while the light areas were larger grains of $L1_2$ modified Al_3Ti which were essentially devoid of TiB_2 [8, 11]. Occasionally, porosity from incomplete densification was seen (Fig. 5b) and all surfaces exhibited damage from EDM in the form of shallow cracks (Fig. 5a).

4. Discussion

Based on the two curves ($Al_{66}Ti_{25}Cr_{4.5}Mn_{4.5}$ and $Al_{66}Ti_{25}Fe_{4.5}Mn_{4.5}$) in Fig. 1, which typify the compressive yield behaviour for the IM quaternary matrices, the XD™, PM processed materials retain a yield strength advantage to $\sim$ 1175 K; thereupon all versions of the quaternaries seem to possess similar strengths. Fig. 6 presents a similar comparison where the 1000 K flow stress–strain rate properties of all four XD™ particulate containing alloys are contrasted with two IM particle-free versions [2]. The behaviour of these latter two materials is representative of the strongest ($Al_{66}Ti_{25}Fe_{4.5}Mn_{4.5}$) and weakest ($Al_{66}Ti_{25}Cr_{4.5}Mn_{4.5}$) matrices. Over the current range of testing, Fig. 6 indicates that

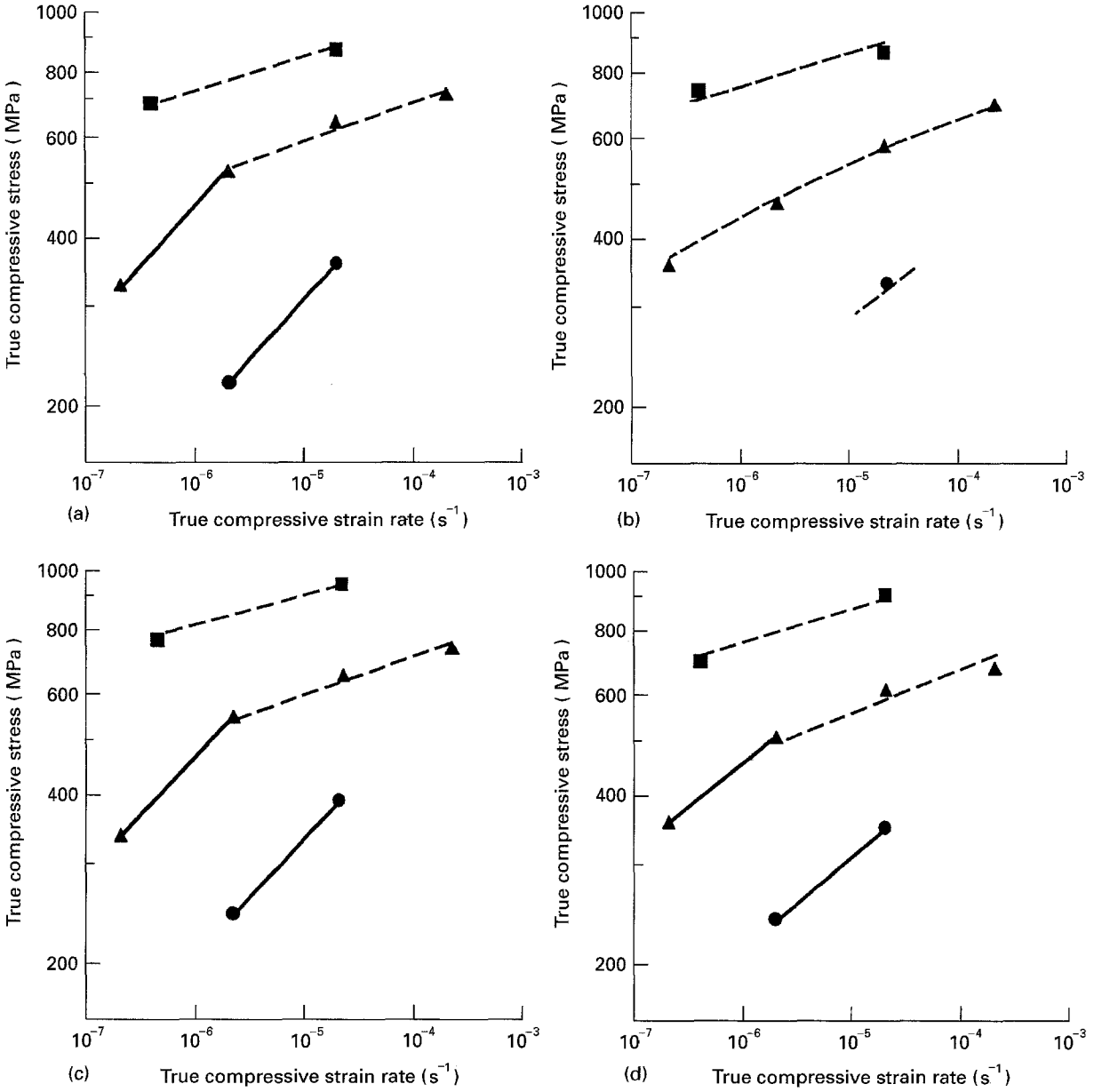

Figure 4 True compressive stress–strain rate behaviour for the composites tested at (■) 900, (▲) 1000, and (●) 1100 K: (a) $Al_{66}Ti_{25}Cr_{4.5}Fe_{4.5}$ + 20 TiB_2, (b) $Al_{66}Ti_{25}Cr_{4.5}Mn_{4.5}$ + 20 TiB_2, (c) $Al_{66}Ti_{25}Fe_{4.5}Mn_{4.5}$ + 20 TiB_2, and (d) $Al_{66}Ti_{25}Mn_{6.7}Fe_{2.3}$ + 20TiB_2.

TABLE I Temperature compensated power law and temperature compensated exponential law fits of the flow stress – strain rate data for several $L1_2$ based Al_3Ti alloys reinforced with 20 vol % TiB_2 particles

Matrix	$B(s^{-1})$	n	$Q(kJ\,mol^{-1})$	R_d^2	δ_n	$\delta_Q(kJ\,mol^{-1})$
(a) Temperature compensated power law[a]						
$Al_{66}Ti_{25}Cr_{4.5}Fe_{4.5}$	22.0	4.79	384.2	0.999	0.17	9.5
$Al_{66}Ti_{25}Fe_{4.5}Mn_{4.5}$	0.738	4.91	363.5	0.999	0.20	10.4
$Al_{66}Ti_{25}Mn_{6.7}Fe_{2.3}$	0.827	6.33	434.2	0.999	0.28	13.7
(b) Temperature compensated exponential law[b]						
$Al_{66}Ti_{25}Cr_{4.5}Fe_{4.5}$	2.14×10^{10}[c]	0.0231[d]	408.5	0.993	0.0016	26.4
$Al_{66}Ti_{25}Cr_{4.5}Mn_{4.5}$	3.99×10^{16}[c]	0.0214[d]	511.3	0.973	0.0018	44.4
$Al_{66}Ti_{25}Fe_{4.5}Mn_{4.5}$	8.23×10^{15}[c]	0.0225[d]	513.9	0.974	0.0029	60.5
$Al_{66}Ti_{25}Mn_{6.7}Fe_{2.3}$	1.74×10^{14}[c]	0.0219[d]	470.2	0.963	0.0034	67.2
(c) Temperature compensated power law[e]						
$Al_{66}Ti_{25}Cr_{4.5}Fe_{4.5}$	2.36×10^{-27}	15.2	395.6	0.974	2.0	49.6
$Al_{66}Ti_{25}Cr_{4.5}Mn_{4.5}$	1.81×10^{-10}	10.8	468.4	0.900	1.9	82.6
$Al_{66}Ti_{25}Fe_{4.5}Mn_{4.5}$	5.32×10^{-25}	16.4	507.4	0.983	1.7	47.9
$Al_{66}Ti_{25}Mn_{6.7}Fe_{2.3}$	2.05×10^{-22}	14.9	466.1	0.977	1.8	52.4

[a] Applied to the higher temperature – slower strain rate data in Fig. 4 (fit illustrated by continuous line).
[b] Applied to the lower temperature – faster strain rate data in Fig. 4 (fit illustrated by dashed line).
[c] Data given is for constant C.
[d] Data given is for constant D.
[e] Applied to the lower temperature – faster strain rate data in Fig. 4 (fit not shown in this figure).

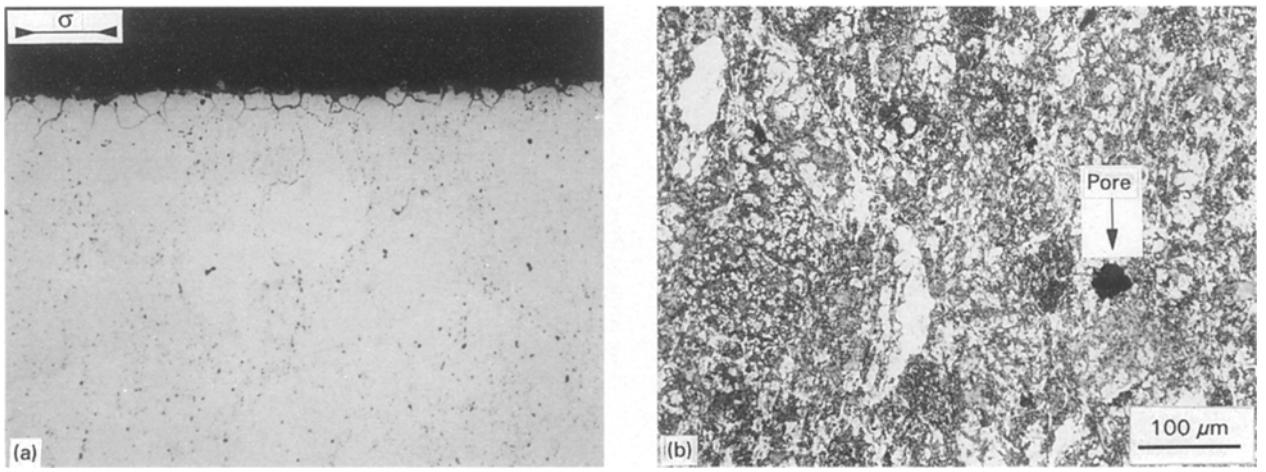

Figure 5 Typical microstructures for the four quaternary $L1_2$ matrix composites containing 20 vol % TiB_2 particles: (a) Al_{66} Ti_{25} $Mn_{6.7}$ $Fe_{2.3}$ + 20 TiB_2 tested at 1100 K at 2.1×10^{-6} s^{-1} to 7% strain and (b) Al_{66} Ti_{25} $Fe_{4.5}$ $Mn_{4.5}$ + 20 TiB_2 tested at 1000 K at 2.1×10^{-7} s^{-1} to 1.5% strain.

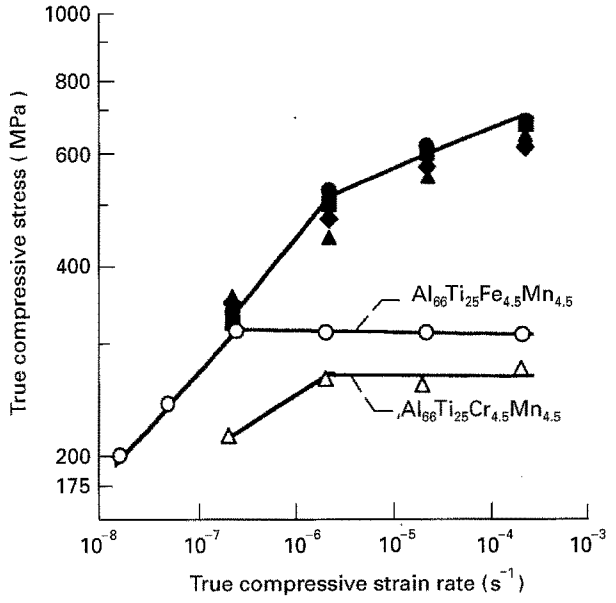

Figure 6 Comparison of the 1000 K true compressive stress–strain rate behaviour of the four quaternary $L1_2$ matrix composites containing 20 vol % TiB_2 particles to ingot metallurgy versions of two matrices [12]. The curve for Al_{66} Ti_{25} $Cr_{4.5}$ $Mn_{4.5}$ + 20 TiB_2 is used to designate composite behaviour: (■) Al_{66} Ti_{25} $Cr_{4.5}$ $Fe_{4.5}$ + 20 TiB_2, (▲) Al_{66} Ti_{25} $Cr_{4.5}$ $Mn_{4.5}$ + 20 TiB_2, (●) Al_{66} Ti_{25} $Fe_{4.5}$ $Mn_{4.5}$ + 20 TiB_2, (♦) Al_{66} Ti_{25} $Mn_{6.7}$ $Fe_{2.3}$ + 20 TiB_2.

1. none of the four quaternary $L1_2$ modified Al_3Ti based materials reinforced with 20 vol % TiB_2 particles has a strength advantage over the others, and

2. all are stronger than the IM alloys. However, visual extrapolation of the data clearly suggests that the particulate reinforced materials will probably not be any stronger than IM Al_{66} Ti_{25} $Fe_{4.5}$ $Mn_{4.5}$ alloy at the lower strain rates of interest for applications.

Comparisons of the 900 and 1100 K true compressive stress–strain rate data for the IM matrices and their TiB_2 reinforced counterparts is given in Fig. 7. Although the existing experimental results for both the composites and unreinforced matrices are limited

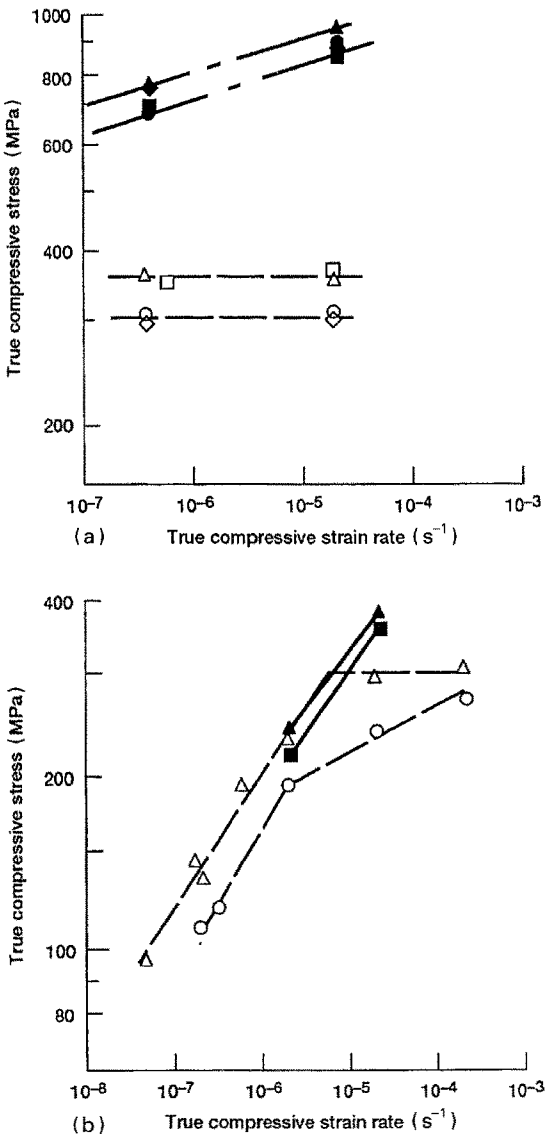

Figure 7 Comparison of the true compressive stress–strain rate behaviour of the quaternary $L1_2$ matrix composites containing 20 vol % TiB_2 particles to ingot metallurgy versions of the matrices [12]: (a) 900 K, and (b) 1100 K. Open symbols represent the IM materials while the filled symbols portray the composites: (□ ■) $Al_{66}Ti_{25}Cr_{4.5}Fe_{4.5}$, (◇ ◆) $Al_{66}Ti_{25}Cr_{4.5}Mn_{4.5}$, (△ ▲) $Al_{66}Ti_{25}Fe_{4.5}Mn_{4.5}$, (○ ●) $Al_{66}Ti_{25}Mn_{6.7}Fe_{2.3}$.

at these temperatures, behaviour follows the tendencies demonstrated by the 1000 K tests (Fig. 6). At 900 K (Fig. 7a) the presence of TiB_2 leads to significant strengthening over the current range of testing; however, the data suggest that the TiB_2 reinforced materials eventually will lose their advantage at lower strain rates. Such a loss of strength is clearly evident at 1100 K (Fig. 7b), where all forms have about the same resistance to deformation at $2 \times 10^{-6}\ s^{-1}$. Taken together, Figs 6 and 7 reveal that incorporation of small TiB_2 particles by the current technology does not appear to be a useful technique to provide high temperature creep strength in $L1_2$ modified Al_3Ti based alloys.

The inability of the TiB_2 particulate reinforcement to improve the creep properties probably lies in the grain structure of the materials. First, Kumar *et al.* [8] demonstrated that decreasing the grain size in PM Cr modified Al_3Ti leads to significant improvement in yield strength up to 1100 K, i.e. an alloy with ~ 4 μm grain size had a yield strength two and a half times greater than the 30 μm version. Second, comparison [12] of 1200 K creep properties of several $L1_2$ modified Al_3Ti alloys revealed that large grain sizes were necessary for good strength. Thus, the small grain size of the $L1_2$ matrix in the TiB_2 enriched regions of current materials provides considerable strengthening at lower temperatures and faster deformation rates (Figs 1, 6 and 7); however, under higher temperature, slower strain rate conditions the same small grains will likely lead to weakening. The true test of the effectiveness of TiB_2 particles in $L1_2$ modified Al_3Ti matrices to produce creep strength awaits the fabrication of large grain size materials. Of course, such alloys will not display the huge increases in lower temperature properties exhibited by the current small grain sized particulate reinforced alloys.

At present it is not clear why TiB_2 particles via XD™ synthesis provide effective creep resistance in B2 ordered NiAl base composites [9] but not in those based on $L1_2$ modified Al_3Ti. Besides the obvious difference in the crystal structure of the matrices, both systems have like microstructures with larger particle-free grains being surrounded by mantles composed of micrometre–submicrometre sized TiB_2 and matrix grains. In addition, creep testing of the composites has been undertaken at a similar range of homologous temperatures from 0.6 to 0.75. At present one can think of only two reasonable explanations for the differences in creep behaviour between NiAl and $L1_2$ modified Al_3Ti reinforced with TiB_2. One possibility lies in basic power law deformation mechanisms of the matrices, and the other possibility involves the inhibition of grain boundary vacancy sinks–sources.

Power law creep in NiAl [14] involves the formation of subgrains, and this alloy can be strengthened by restricting the grain size to be less than the equilibrium subgrain size [15]. Therefore, the small grain size XD™ NiAl–TiB_2 composites can help to promote creep strength [9]. On the other hand, even though subgrains have been seen in $L1_2$ modified Al_3Ti [6], it has not been demonstrated that subgrains are an important factor in the creep of these materials. If creep in $L1_2$ modified Al_3Ti does not directly involve the formation of subgrains, then decreasing the grain size of the matrix is unlikely to lead to strengthening and might, instead, lead to weakening via diffusion creep mechanisms. The potential for diffusion creep suggests the second possible difference between $L1_2$ modified Al_3Ti and NiAl matrix particulate composites. In this instance it can be envisioned that TiB_2 particles (or dissolved Ti/B) on grain boundaries influence the capability of boundaries to absorb or create vacancies. If TiB_2 particles grossly decrease the action of vacancy sinks–sources in NiAl, but have little influence on their response in $L1_2$ modified Al_3Ti, diffusion creep mechanisms would lead to weakening in the $L1_2$ modified materials, but not NiAl. While each of these two explanations can individually explain the difference between the TiB_2 reinforced NiAl and $L1_2$ modified Al_3Ti composites, it is possible that both mechanisms could be operating simultaneously.

5. Conclusions

Compression testing of four XD™ synthesized, powder metallurgy processed quaternary $L1_2$ modified Al_3Ti based materials reinforced with 20 vol % TiB_2 particles has been undertaken as functions of temperature and strain rate. Within the limits of current testing, the particulate reinforced materials are generally stronger than the ingot metallurgy matrices. However, extrapolation of the current data to slow strain rate regimes indicates that the composites will not possess any strength advantage. Such a loss in strength appears to be a grain size effect.

References

1. K. S. KUMAR and C. T. LIU, *J. Mater.* **45** (1993) 28.
2. Y. NAKAYAMA and H. MABUCHI, *Intermetallics* **1** (1993) 41.
3. L. J. PARFITT, J. M. SMIALEK, J. P. NIC and D. E. MIKKOLA, *Scripta Metall. Mater.* **25** (1991) 727.
4. K. S. KUMAR and S. A. BROWN, *Philos. Mag. A* **65** (1992) 91.
5. S. A. BROWN, K. S. KUMAR and J. D. WHITTENBERGER, *Scripta Metall. Mater.* **24** (1990) 2001.
6. M. S. DIPIETRO, K. S. KUMAR and J. D. WHITTENBERGER, *J. Mater. Res.* **6** (1991) 530.
7. J. D. WHITTENBERGER, K. S. KUMAR, S. BROWN, M. S. DIPIETRO and S. C. FARMER, in "Light Weight Alloys for Aerospace Applications II", edited by E. W. Lee and N. J. Kim (TMS, Warrendale, PA, 1991) pp. 327–349.
8. K. S. KUMAR, M. S. DIPIETRO and J. D. WHITTENBERGER, *Acta Metall. Mater.* **41** (1993) 1379.
9. J. D. WHITTENBERGER, R. K. VISWANANDHAM, S. K. MANNAN and B. SPRISSLER, *J. Mater. Sci.* **25** (1990) 35.
10. K. S. KUMAR and S. A. BROWN, *Scripta Metall.* **26** (1992) 197.
11. K. S. KUMAR, M. S. DIPIETRO, S. BROWN and J. D. WHITTENBERGER, NASA TM 105628 (1992).
12. J. D. WHITTENBERGER, K. S. KUMAR, M. S. DIPIETRO and S. BROWN, *Intermetallics.* **3** (1995) 221.
13. K. S. KUMAR, M. S. DIPIETRO, S. BROWN and J. D. WHITTENBERGER, NASA TM 103724 (1991).
14. R. D. NOEBE, R. R. BOWMAN and M. V. NATHAL, *Inter. Mater. Rev.* **38** (1993) 193.
15. J. D. WHITTENBERGER, *J. Mater. Sci.* **23** (1988) 35.

Received 18 July 1994
and accepted 11 April 1995